Check for updates

Geophysical Research Letters

RESEARCH LETTER
10.1029/2024GL111703

Characteristics of Tropical Cyclone Outer Size and Structure Associated With Extratropical Transition

Dzuy Nguyen[1,2,3] **and Benjamin A. Schenkel**[1,2,4]

[1]School of Meteorology, University of Oklahoma, Norman, OK, USA, [2]Cooperative Institute for Severe and High-Impact Weather Research and Operations, Norman, OK, USA, [3]Now at Tinker Air Force Base, Norman, OK, USA, [4]NOAA/OAR National Severe Storms Laboratory, Norman, OK, USA

Key Points:

- Tropical cyclone outer size and structure do not typically change until after extratropical transition
- Tropical cyclone outer winds broaden and become asymmetric in the lower troposphere first for cases that strongly expand during transition
- Those cases that strongly expand are smaller at transition start and become embedded in strongly baroclinic environments by transition end

Supporting Information:

Supporting Information may be found in the online version of this article.

Correspondence to:

B. A. Schenkel,
benschenkel@gmail.com

Citation:

Nguyen, D., & Schenkel, B. A. (2025). Characteristics of tropical cyclone outer size and structure associated with extratropical transition. *Geophysical Research Letters*, *52*, e2024GL111703. https://doi.org/10.1029/2024GL111703

Received 5 AUG 2024
Accepted 17 DEC 2024

Abstract There is a lack of consensus on how tropical cyclone outer winds may change, if at all, due to extratropical transition. Hence, this study examines changes in North Atlantic tropical cyclone outer size and structure using a large, multidecadal sample of cases from reanalysis data. These results suggest that tropical cyclone outer size and structure typically remain unchanged until after extratropical transition end. In those minority of cases with strong expansion during extratropical transition, increases in tropical cyclone outer winds begin first in the lower troposphere during extratropical transition and build upwards over time. This broadening of the azimuthal-mean outer winds is also associated with an increasingly asymmetric outer wind field with the strongest winds concentrated downstream of the tropical cyclone. These storms that expand most strongly during transition are typically smaller at transition start and eventually become embedded in more strongly baroclinic environments by extratropical transition end.

Plain Language Summary Tropical cyclones (also known as hurricanes, typhoons, cyclones, tropical storms, and tropical depressions) undergo major structural changes when transforming into an extratropical cyclone (non-tropical low-pressure system) during a process known as extratropical transition. An understudied aspect of these structure changes is the response of the tropical cyclone outer winds to extratropical transition. Hence, this study investigates how the structure and size of the tropical cyclone outer wind field will change in response to extratropical transition for a large sample of cases. These results show that tropical cyclone outer winds typically do not change until after extratropical transition. In the minority of cases with strong expansion in tropical cyclone outer winds during transition, we show a broadening of the outer wind field that begins in the lower troposphere (i.e., the lowest part of the atmosphere) during extratropical transition that deepens with time. This broadening of the outer wind field is associated with an increasingly asymmetric wind field whose maximum is concentrated in the direction in which the tropical cyclone is propagating. These cases that expand typically are smaller at extratropical transition start and become embedded in environments with strong horizontal and vertical variations in winds, temperature, and moisture by extratropical transition end.

1. Introduction

North Atlantic tropical cyclones (TCs) occasionally landfall in the midlatitudes causing compound hazards including flooding and tornadoes (Galarneau et al., 2013; Schenkel et al., 2020). Approximately 50% of land-falling TCs along the United States East Coast, Canada, and Europe eventually undergo extratropical transition (ET; Hart & Evans, 2001). ET is the process by which a TC becomes an extratropical cyclone upon typically encountering increasing baroclinicity, decreasing sea surface temperatures or making landfall, and interaction with an upper-tropospheric trough (Evans et al., 2017; Jones et al., 2003). The associated transition to baroclinic energetics leads to the post-ET re-intensification in 50% of TCs, yielding the landfall of damaging extratropical cyclones (Bieli et al., 2019a; Hart & Evans, 2001). Moreover, climate projections suggest increasing numbers of more intense ET events with more landfalls in western Europe later this century due to anthropogenic warming (Haarsma et al., 2013; Liu et al., 2017). These projected changes in ET frequency and location necessitate a complete understanding of ET-induced TC structure changes to better anticipate their associated hazards.

TC outer winds are a key element impacting the magnitude and area of hazards like storm surge and tornadoes (Lin et al., 2014; Paredes et al., 2021). Indeed, damage is more strongly related to metrics accounting for TC intensity and outer size than intensity alone (Chavas et al., 2017; Klotzbach et al., 2020). However, previous studies have primarily focused on TC inner-core winds, which typically broaden and weaken during ET (Loridan

© 2025. The Author(s).
This is an open access article under the terms of the Creative Commons Attribution License, which permits use, distribution and reproduction in any medium, provided the original work is properly cited.

19448007, 2025, 5, Downloaded from https://agupubs.onlinelibrary.wiley.com/doi/10.1029/2024GL111703 by University Of Oklahoma, Wiley Online Library on [04/03/2025]. See the Terms and Conditions (https://onlinelibrary.wiley.com/terms-and-conditions) on Wiley Online Library for rules of use; OA articles are governed by the applicable Creative Commons License

et al., 2014; Quinting et al., 2014). However, TC outer size varies largely independently of intensity given that outer radii are characterized by comparatively weaker winds, sparser convection, and differing energetics (i.e., radiative-subsidence balance; Weatherford & Gray, 1988; Chavas et al., 2015), which motivates a separate study.

Our knowledge of the TC outer size life cycle before ET has been well studied with the smallest sizes at genesis (Chan & Chan, 2018; Schenkel et al., 2018). After that, outer size gradually increases throughout most of the North Atlantic TC life cycle (Merrill, 1984; Schenkel et al., 2018). The largest TCs tend to be longer-lived, while traversing the greatest distances (e.g., recurving into midlatitudes) suggesting that outer size expands during ET (Cocks & Gray, 2002; Schenkel et al., 2018). However, there remains disagreement among prior work as to whether lower-tropospheric TC outer size typically expands (Evans & Hart, 2008; Hart et al., 2006) or remains unchanged during ET (Schenkel et al., 2018). Theory as given by the Rhines scale suggests that the TC outer size distribution should shift toward larger values during ET in association with a stronger Coriolis parameter and greater ambient relative vorticity accompanying ambient baroclinicity. In those cases where TC outer size increases during ET, expansion may begin in the midtroposphere due to the enhanced imports of absolute angular momentum associated with warm conveyor belt development as shown in a case study of Hurricane Bonnie (1998) by Evans and Hart (2008).

Together, these studies suggest that our understanding of TC outer wind size and structure during ET remains incomplete. Hence, this study investigates how the TC outer wind field changes throughout the troposphere during and after ET using a large sample of cases. Specifically, we use multidecadal reanalysis data to quantify changes in TC outer wind field size and structure. This work addresses the following questions:

- Does TC outer size typically increase due to ET?
- When and in what part of the TC do outer wind field changes first occur in association with ET?
- What TC and environmental factors are associated with outer wind expansion?

2. Data and Methods

2.1. TC Track Data

North Atlantic TC track data from 1979 to 2020 are obtained from the National Hurricane Center HURricane DATabase, version 2 (HURDAT2; Landsea & Franklin, 2013). Our analysis focuses on those TCs that: (a) attained at least tropical depression strength and (b) completed ET in HURDAT2. All TCs that undergo ET in HURDAT2 are tracked until their cyclolysis (C. Landsea, personal communication, 22 March 2022).

2.2. TC Outer Wind Data

TC outer wind field data are sourced from 6-hr $0.25° \times 0.25°$ fifth-generation ECMWF reanalysis data (ERA-5; Hersbach et al., 2020). Here we isolate the TC winds as the irrotational and nondivergent components within a 500-km distance from the TC computed by solving a Poisson equation using uniform boundary conditions (Davis et al., 2008; Galarneau & Davis, 2013). While reanalyses underestimate TC intensity and its life cycle (Hodges et al., 2017; Schenkel & Hart, 2012), ERA-5 TC outer size and structure throughout the troposphere are comparable to observations (Bian et al., 2021; Slocum et al., 2022). Moreover, the ERA-5 represents the timing and structure changes of ET well compared to observations (Sarro & Evans, 2022).

Nontrivial uncertainties are associated with TC location in both HURDAT2 (Landsea & Franklin, 2013; Torn & Snyder, 2012) and reanalyses (Murakami, 2014; Schenkel & Hart, 2012). Hence, this study uses an objective TC recentering algorithm, based upon the GFDL vortex tracker (Brammer, 2017; Marchok, 2002): (a) using the HURDAT2 TC center location as the first guess and (b) then compute the final TC location as the mean of the centers of mass of 925-hPa, 850-hPa, and 700-hPa relative vorticity, 850-hPa and 700-hPa geopotential height, and mean sea-level pressure around the first guess.

2.3. TC Outer Size Data

We employ an axisymmetric TC outer size metric defined as the radius at which the azimuthal-mean azimuthal TC wind speed equals 6 m s^{-1} (r_6) derived from the ERA-5. Schenkel et al. (2017) and Bian et al. (2021) have shown that r_6 is more frequently defined than other metrics (e.g., r_8) and is particularly well represented in reanalyses. We use reanalysis data rather than the HURDAT2 radius of 17 m s^{-1} 10-m winds (R17) estimates

19448007, 2025, 5, Downloaded from https://agupubs.onlinelibrary.wiley.com/doi/10.1029/2024GL111703 by University Of Oklahoma, Wiley Online Library on [04/03/2025]. See the Terms and Conditions (https://onlinelibrary.wiley.com/terms-and-conditions) on Wiley Online Library for rules of use; OA articles are governed by the applicable Creative Commons License

since the latter is subjective, method dependent, and prone to uncertainty as discussed in Section 5 of the Supporting Information S1 (Knaff et al., 2014; Landsea & Franklin, 2013). We compute r_6 at each isobaric level from 1,000 hPa to 100 hPa at 25–50-hPa increments (i.e., ERA-5 isobaric output grid) following Chavas and Vigh (2014):

1. Interpolating the wind field at a given isobaric level to a TC-centered polar coordinate using the objectively identified reanalysis TC location, and removing data below the surface;
2. Partition the TC winds from the total winds by solving a Poisson equation using uniform boundary conditions within a 500-km distance of the TC (Davis et al., 2008; Galarneau & Davis, 2013);
3. Calculate the azimuthal-mean azimuthal TC winds;
4. Interpolate the radial profile of these azimuthal-mean winds to a grid spacing equivalent to ≈0.5 times the ERA-5 horizontal output grid;
5. Identify r_6 from the radial profile as the first point outside the radius of maximum wind where the azimuthal-mean azimuthal wind equals 6 m s^{-1}.

We remove a horizontally and vertically varying ambient wind rather than subtracting out TC motion since the latter assumes weak horizontal and vertical wind field variations that are atypical of ET cases (Klein et al., 2000; Thorncroft et al., 1993). Undefined r_6 values may exist where isobaric levels fall below ground (Chavas & Vigh, 2014) or when a reanalysis TC is too weak to identify. Part of our analysis will bin TCs into terciles based upon the difference in r_6 between ET start and end, which is quasi-Gaussian with a mean of approximately 0 and a longer right tail (see Figure S1 of the Supporting Information S1) to help identify cases that strongly contract (i.e., first tercile of outer size change) versus those that strongly expand (i.e., third tercile) during ET. Hereafter, we refer to these two groups as the "contraction" and "expansion" groupings without the use of "strongly" in the interest of brevity although both show substantial size changes. The expansion group is associated with TCs that impact the United States east coast more frequently relative to the contraction group (Figure S2 of the Supporting Information S1). Focus is placed on the 925-hPa level given this is where TC winds before and during ET are maximized (Abraham et al., 2004; Franklin et al., 2003).

2.4. ET Definition

Given that HURDAT2 only provides the ET end time, this study applies cyclone phase space diagnostics to ERA-5 data to objectively compute ET start and end times for ET events in HURDAT2 (Hart, 2003). The first metric is the lower-tropospheric thermal asymmetry parameter (i.e., B), which quantifies TC frontal structure. This parameter is computed as the difference between the 900–600-hPa layer thickness to the left-and right-of-TC motion. ET start is defined when this parameter is greater than an empirically defined value of 10 m (Hart, 2003). The second parameter is the lower-tropospheric thermal wind (i.e., $-V_L^T$), which quantifies whether the TC is a warm-core or cold-core cyclone in the 900–600-hPa layer. Together, these parameters define two potential types of ET: (a) frontal, cold-core extratropical cyclones ($B > 10$, $-V_L^T < 0$) and (b) frontal, warm-core (i.e., warm-seclusion) extratropical cyclones ($B > 10$, $-V_L^T > 0$). Here we exclude ET cases that acquire cold-core structure before becoming frontal due to the rarity of the cases in the ERA-5 (8 TCs), our lack of understanding of their structure and energetics, and the potential uncertainty with the underrepresentation of the TC warm core in these cases (Bieli et al., 2019b; Sarro & Evans, 2022; Schenkel & Hart, 2012).

ET start for both pathways is diagnosed when the TC retains its warm core $\left(-V_L^T > 0\right)$ while transforming from a non-frontal ($B \leq 10$) to a frontal cyclone ($B > 10$). ET end for cold-core extratropical cyclones is defined when the TC remains frontal ($B > 10$) while becoming cold core $\left(-V_L^T < 0\right)$. All cold-core extratropical cyclone ET events diagnosed by the cyclone phase space with ≥18 hr disagreement with the HURDAT2 ET end time are excluded from the analysis following Sarro and Evans (2022). Defining ET end for warm-seclusion extratropical cyclones involves identifying TCs that retain warm core and frontal characteristics through at least 12 hr before and after the HURDAT2 ET end time. This is followed by subjective examination of satellite data and ERA-5-derived kinematic and thermodynamic data, similar to Sarro and Evans (2022). These criteria yield a total of 139 TCs that undergo ET with the difference between the timing of ET end from HURDAT2 versus the cyclone phase space applied to the ERA-5 shown in Figure S3 of the Supporting Information S1.

19448007, 2025, 5, Downloaded from https://agupubs.onlinelibrary.wiley.com/doi/10.1029/2024GL111703 by University Of Oklahoma, Wiley Online Library on [04/03/2025]. See the Terms and Conditions (https://onlinelibrary.wiley.com/terms-and-conditions) on Wiley Online Library for rules of use; OA articles are governed by the applicable Creative Commons License

2.5. Environmental and TC Diagnostics

Our analysis examines whether any differences exist between the characteristics of TCs and their environments between the subset of cases with expansion and contraction during ET. To quantify thermodynamic environmental favorability for TCs, we examine potential intensity (Bister & Emanuel, 2002; Emanuel, 1986). Potential intensity has been used to quantify the environmental favorability for tropical development in prior ET studies (Hart & Evans, 2001; Sarro & Evans, 2022):

$$p_{\min} = p_{msl} \times \exp\left(\frac{CAPE_{RMW} + \frac{1}{2}\left(1+\frac{1}{b}\right)V_{\max}^2}{R_d T_{v,sfc}}\right) \quad (1)$$

where $p_{\min}$ is the minimum theoretical central pressure, p_{msl} is the environmental mean sea-level pressure, $CAPE_{RMW}$ is the ambient mean sea-level CAPE evaluated at the TC radius of maximum wind, $b = 2$ following Bister and Emanuel (2002), R_d as the specific gas constant of dry air, and $T_{v,sfc}$ as the surface environmental virtual temperature. These calculations use ERA-5 input variables averaged within a 500-km distance of the HURDAT2 track point between 5 and 10 days before TC passage to reduce TC self-contamination (Hart et al., 2007; Schenkel & Hart, 2015a, 2015b).

To determine ambient favorability for baroclinic development, we use the 700-hPa Eady growth rate calculated from ERA-5 data (Hoskins & Valdes, 1990):

$$\sigma = 0.31 f \left\| \frac{\partial \mathbf{v}}{\partial z} \right\| N^{-1} \quad (2)$$

where f is the Coriolis parameter, $\left\|\frac{\partial \mathbf{v}}{\partial z}\right\|$ is the vertical wind shear magnitude, and N is the Brunt-Väisälä frequency calculated at 700 hPa. Each term is calculated as the average value within a 500-km radius of the reanalysis TC track point at ET start and end following Yanase et al. (2020). Additionally, we also examine TC intensity and r_6 at ET start and end.

2.6. Statistical Testing

We objectively test differences between distributions using a bootstrap approach for a two-tailed test at the 10% and 5% levels in the time series and joint histograms shown later. Specifically, we randomly select ET cases (with replacement) to construct a distribution, compute a median value, and repeat the process to obtain 10,000 medians to estimate significance levels. Where possible, plots with bootstrapping utilized p-values defined using a false discovery rate with values of $\alpha = 0.2$ and $\alpha = 0.1$, which correspond to 10% and 5% global significance levels, respectively (Benjamini & Hochberg, 1995; Ventura et al., 2004).

3. Results

3.1. Azimuthal-Mean Outer Size

Most TCs show no significant changes in lower and midtropospheric outer size until after ET end as suggested by no significant differences in Figure 1 until then. This result agrees with the climatology of Schenkel et al. (2018), while contradicting other studies whose conclusions remain uncertain given their focus on case studies or results showing similarly large increases in the mean and standard deviation of outer size during ET (Evans & Hart, 2008; Hart et al., 2006). However, there is a subset of TCs that expand during ET as suggested by significant increases ($p < 0.05$) in the 75th percentile of 925-hPa r_6 from 863 km at ET start to 992 km at ET end. This subset of cases first show significant r_6 increases in the lower troposphere (Figures 1a and 1b) before building upwards (Figure 1c). These conclusions are not an artifact of cases dropping out due to cyclolysis as shown by re-creating Figure 1 using cases that persisted for ≥24 hr after ET end (Figure S4 of the Supporting Information S1).

10.1029/2024GL111703

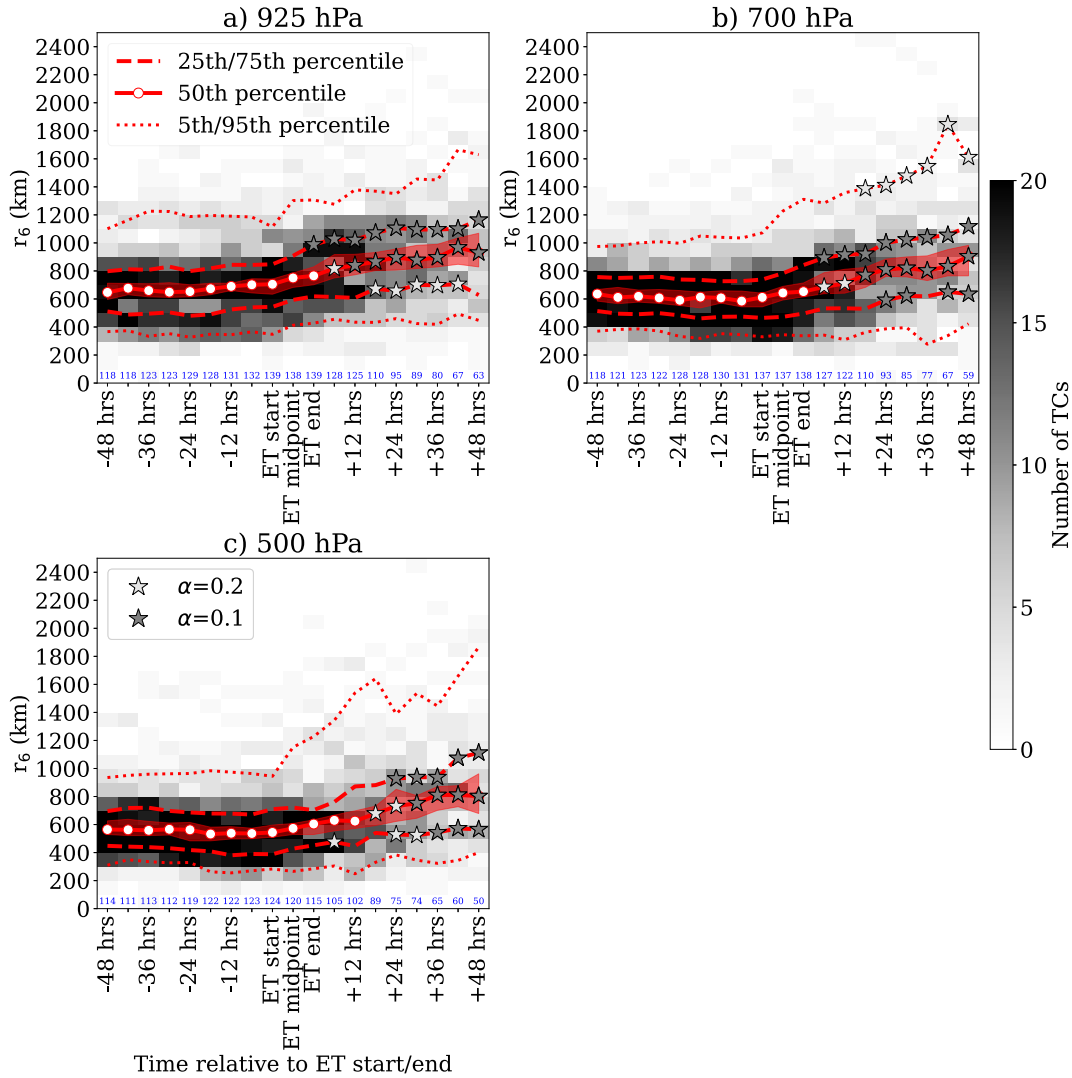

Figure 1. Heat map of hours relative to ET start and end versus r_6 (km) at (a) 925 hPa, (b) 700 hPa, and (c) 500 hPa. The red solid line, shading, dashed lines, and dotted lines show the median, 95% confidence interval, 25th and 75th percentiles, and 5th and 95th percentiles, respectively. Stars show when either the time series of the 5th, 25th, 50th, 75th, or 95th percentiles of r_6 for a given time bin is significantly different from r_6 at ET start using bootstrapping with p-values defined using false discovery rates of $\alpha = 0.2$ (light gray stars) and $\alpha = 0.1$ (dark gray stars).

Figure 2 shows the case-to-case variability in lower-tropospheric outer size changes during and after ET. Specifically, r_6 during ET is initially strongly related to values at ET start ($R = 0.81$; $p < 0.05$ at mid-ET) before significantly decreasing thereafter to moderate correlations by 24 hr after ET end ($R = 0.48$; $p < 0.05$). This weakening of correlations with time after ET start is due to a greater fraction of the smallest TCs at ET start that expand during ET (70% of these cases) compared to the largest TCs (33%). Figure 2 also shows that the majority of the TCs that have been the focus of ET case studies tend to be larger both during and after ET, and potentially suggests that these TCs are atypical of outer size evolution. Last, Figure 2 results are also not sensitive to cases dropping out due to cyclolysis following ET end (see Figure S5 of the Supporting Information S1). Together, the results thus far suggest that most TCs do not expand until after ET end, although those cases that expand during ET are often smaller at ET start. This latter result is the focus of the next section.

3.2. Vertical and Horizontal Structure

Composite vertical cross-sections of azimuthal-mean TC-relative azimuthal (i.e., tangential) winds show that those TCs that strongly expand in outer size during ET first show a strengthening of lower-tropospheric outer

19448007, 2025, 5, Downloaded from https://agupubs.onlinelibrary.wiley.com/doi/10.1029/2024GL111703 by University Of Oklahoma, Wiley Online Library on [04/03/2025]. See the Terms and Conditions (https://onlinelibrary.wiley.com/terms-and-conditions) on Wiley Online Library for rules of use; OA articles are governed by the applicable Creative Commons License

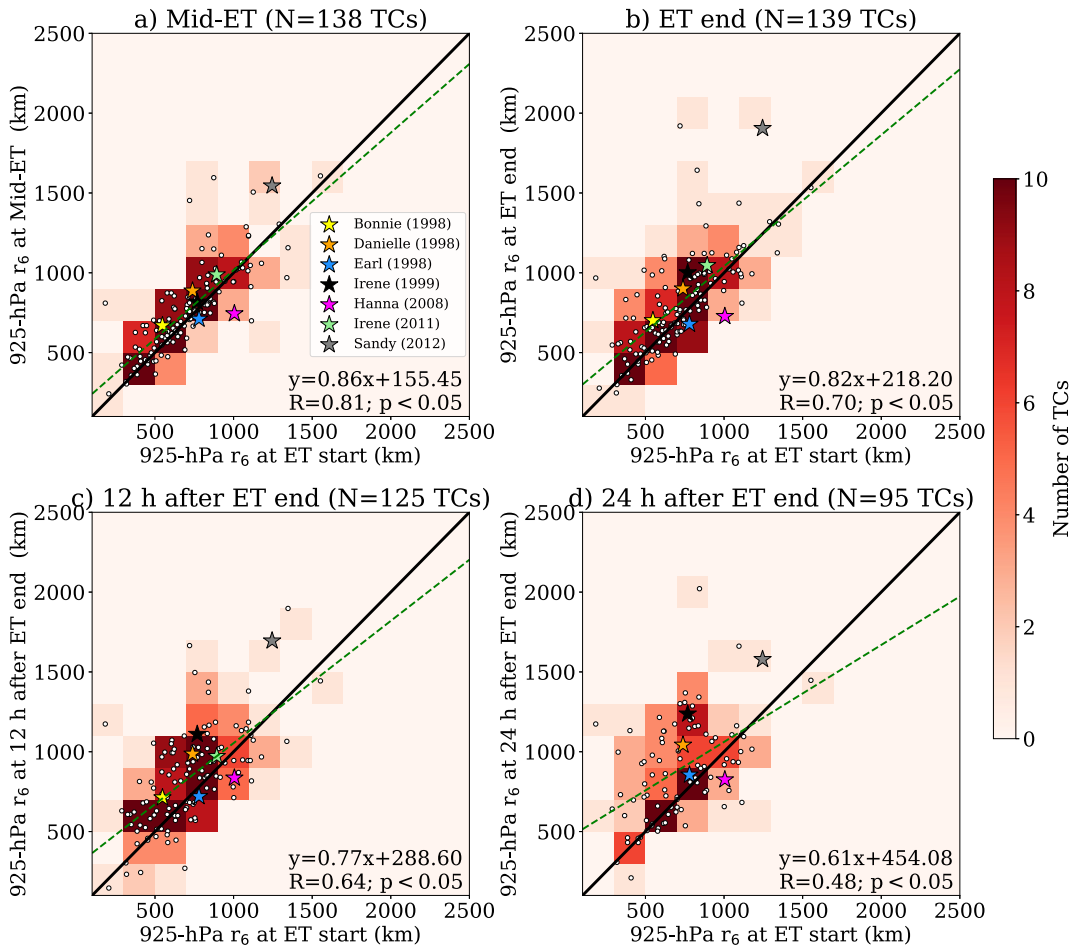

Figure 2. Heat map of 925-hPa r_6 at ET start versus 925-hPa r_6 at (a) mid-ET, (b) ET end, (c) 12 hr after ET end, and (d) 24 hr after ET end. The green dashed line shows the linear least squares regression between the two quantities with its equation, correlation coefficient, and p-value provided. Stars denote selected TCs from previous studies.

winds (Figures 3b, 3d, 3f, and 3h). In particular, significant increases in lower-tropospheric outer winds ($p < 0.05$) first occur at mid-ET with maximum increases of 2.4 m s^{-1} at a distance of $\frac{r}{r_6} \approx 1.0$. After that, outer winds continue to increase in magnitude over a broader region covering $\frac{r}{r_6} \geq 0.5$ with maximum increases of 6.9 m s^{-1} at 24 hr after ET end. These outer wind increases also become deeper with time extending from the lower troposphere into the midtropsphere. This evolution differs from the downward expansion of Hurricane Bonnie (1998) from the midtroposphere shown in Evans and Hart (2008). The expansion subset is also characterized by the weakening of upper-tropospheric anticyclonic winds, which becomes significant ($p < 0.05$) 24 hr after ET end at $r/r_6 > 1.0$. In contrast, the contraction subset shows no significant differences in TC outer winds during or after ET (Figures 3a, 3c, 3e, and 3g).

We next examine the horizontal structure of 925-hPa azimuthal winds (i.e., level where the wind field changes are strongest) in a TC motion-relative coordinate (Figure 4). The broadening of the outer winds for cases in the expansion subset during ET (shown earlier in Figure 3) is associated with the development of asymmetries downstream and to the right of motion. These asymmetries become strongest and most significant ($p < 0.05$) downstream of the TC after ET end. Specifically, Figure S6 of the Supporting Information S1 show that the differences in area-averaged right-of-motion TC winds increase from 0.4 m s^{-1} stronger than left of motion at ET start to 3.0 m s^{-1} at 24 hr after ET end in the expansion subset. Relative to the winds at ET start, these increases are maximized 24 hr after ET end with maximum changes of 10.2 m s^{-1}. This downstream enhancement of TC outer winds is consistent with the location of warm conveyor belt development highlighted by the green circles in

19448007, 2025, 5, Downloaded from https://agupubs.onlinelibrary.wiley.com/doi/10.1029/2024GL111703 by University Of Oklahoma, Wiley Online Library on [04/03/2025]. See the Terms and Conditions (https://onlinelibrary.wiley.com/terms-and-conditions) on Wiley Online Library for rules of use; OA articles are governed by the applicable Creative Commons License

10.1029/2024GL111703

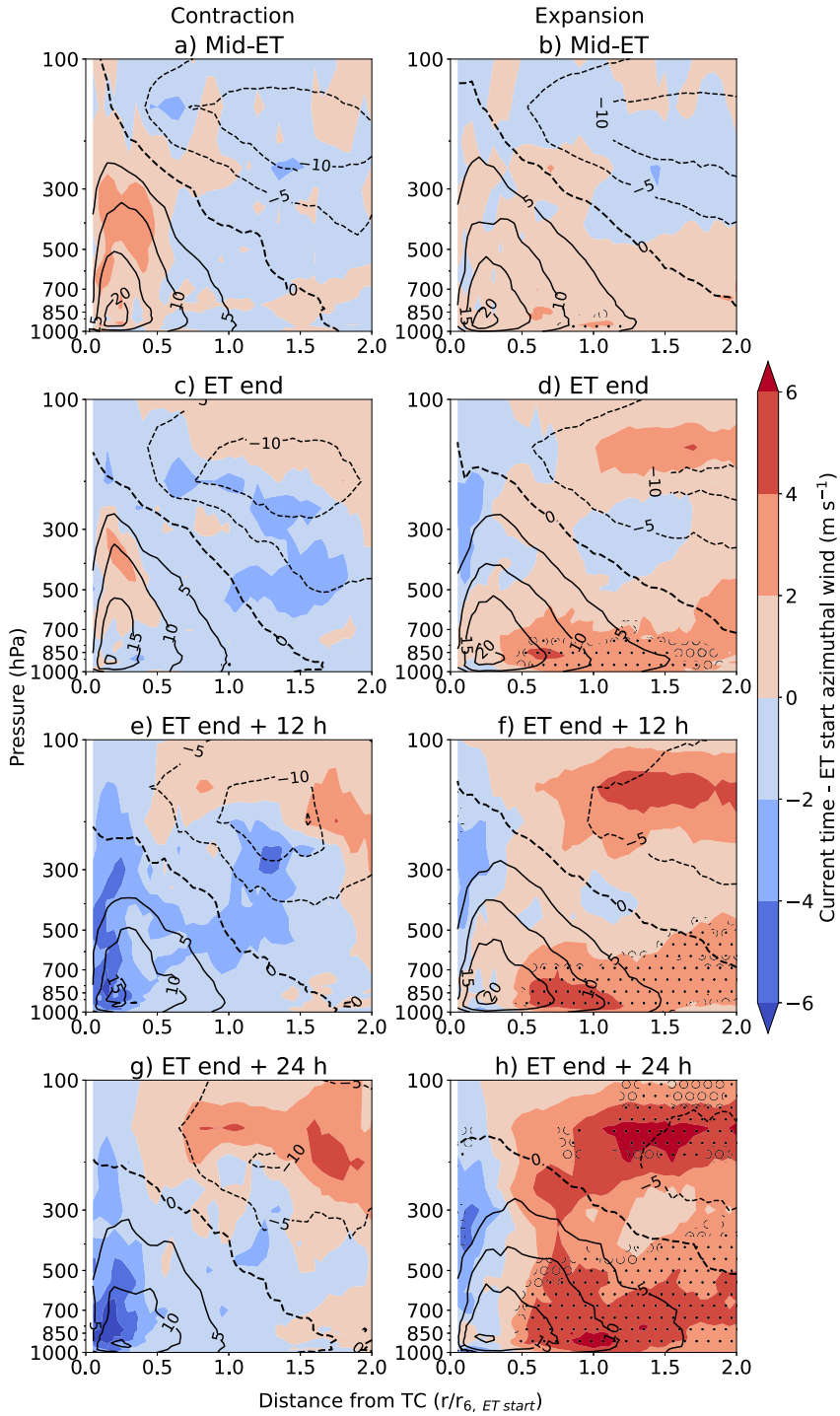

Figure 3. Vertical cross-section showing the median values of the azimuthal-mean TC-relative azimuthal (i.e., tangential) winds (m s^{-1}; black contours) at (a,b) mid-ET, (c,d) ET end, (e,f) ET end + 12 hr, and (g,h) ET end + 24 hr as function of distance from the TC center normalized by r_6 at ET start for the (a,c,e,g) contraction and (b,d,f,h) expansion subsets. Shading shows the difference in azimuthal winds at ET start with the time being considered (m s^{-1}; shading). The unfilled and filled black circles in panels (d,f,h) show grid points where azimuthal wind differences are greater than 0 according to bootstrapping with p-values defined using false discovery rates of $\alpha = 0.2$ and $\alpha = 0.1$, respectively.

19448007, 2025, 5, Downloaded from https://agupubs.onlinelibrary.wiley.com/doi/10.1029/2024GL111703 by University Of Oklahoma, Wiley Online Library on [04/03/2025]. See the Terms and Conditions (https://onlinelibrary.wiley.com/terms-and-conditions) on Wiley Online Library for rules of use; OA articles are governed by the applicable Creative Commons License

10.1029/2024GL111703

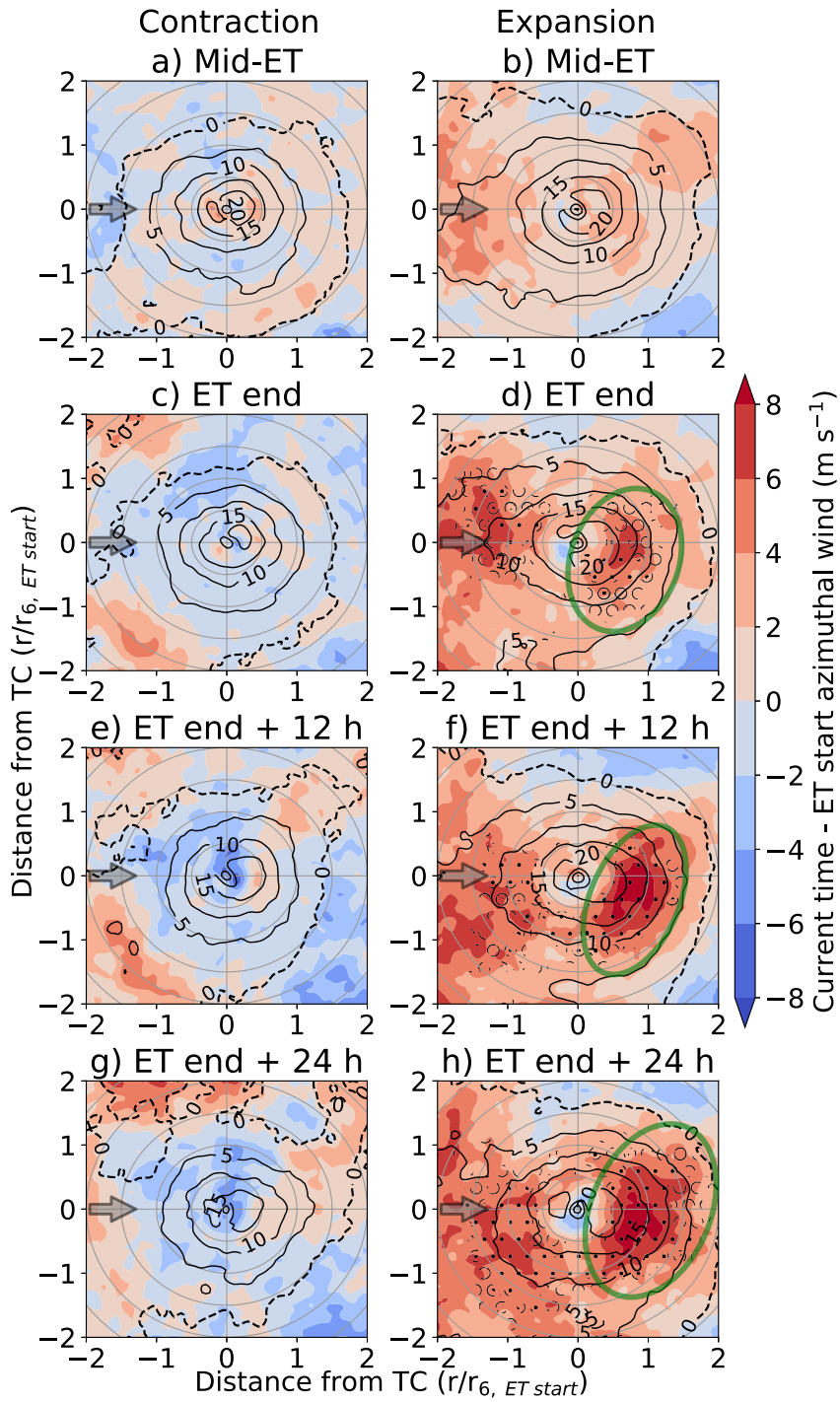

Figure 4. TC motion-relative plan view showing median values of 925-hPa azimuthal winds (m s^{-1}) at (a, b) mid-ET, (c, d) ET end, (e, f) ET end + 12 hr, and (g, h) ET end + 24 as a function of TC distance normalized by r_6 at ET start for the (a, c, e, g) contraction and (b, d, f, h) expansion subsets and their difference with values at ET start (m s^{-1}; shading). The unfilled and filled black circles in panels (d, f, and h) show grid points where azimuthal wind differences are greater than 0 according to bootstrapping with p-values defined using false discovery rates of $\alpha = 0.2$ and $\alpha = 0.1$, respectively. The azimuthal wind field has been rotated around the TC center such that storm motion is pointing to the right (gray vector). The green circles identify the downstream area of greatest TC wind field expansion during and after ET.

19448007, 2025, 5, Downloaded from https://agupubs.onlinelibrary.wiley.com/doi/10.1029/2024GL111703 by University Of Oklahoma, Wiley Online Library on [04/03/2025]. See the Terms and Conditions (https://onlinelibrary.wiley.com/terms-and-conditions) on Wiley Online Library for rules of use; OA articles are governed by the applicable Creative Commons License

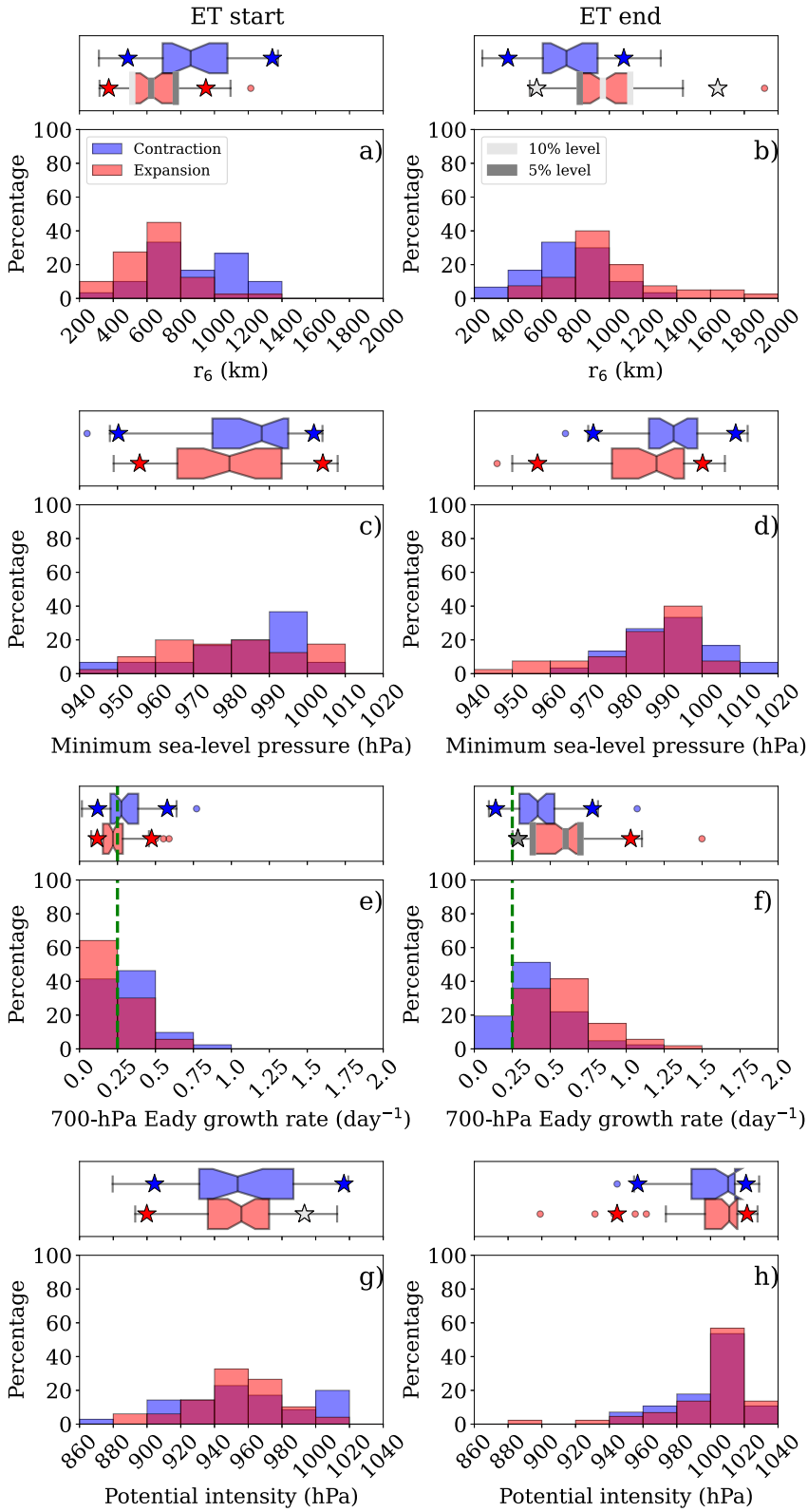

Figure 5.

19448007, 2025, 5, Downloaded from https://agupubs.onlinelibrary.wiley.com/doi/10.1029/2024GL111703 by University Of Oklahoma, Wiley Online Library on [04/03/2025]. See the Terms and Conditions (https://onlinelibrary.wiley.com/terms-and-conditions) on Wiley Online Library for rules of use; OA articles are governed by the applicable Creative Commons License

19448007, 2025, 5, Downloaded from https://agupubs.onlinelibrary.wiley.com/doi/10.1029/2024GL111703 by University Of Oklahoma, Wiley Online Library on [04/03/2025]. See the Terms and Conditions (https://onlinelibrary.wiley.com/terms-and-conditions) on Wiley Online Library for rules of use; OA articles are governed by the applicable Creative Commons License

Figures 4d, 4f, and 4h, which has been hypothesized to be important to size expansion in prior work (Evans & Hart, 2008; Hart, 2003). In contrast, no significant differences occur at any point in the contraction grouping. In summary, TCs that strongly expand in azimuthal-mean outer size tend to do so asymmetrically in the lower troposphere during ET, building upwards and downstream with time.

3.3. TC and Environment Characteristics Favoring Expansion Versus Contraction

We next examine the differences in TC and environmental characteristics between TCs that show expansion and contraction during ET (Figure 5). We only show those variables with either the largest changes or that are most relevant in the interest of brevity. Those TCs that undergo strong expansion during ET tend to have smaller outer sizes at ET start compared to those TCs in the contraction grouping (Figure 5a), with significant differences in the 25th, 50th, and 75th percentiles ($p < 0.05$). These significant differences include median values of 624 km in the expansion grouping versus 840 km in the contraction subset. By ET end, those cases in the expansion subset have expanded sufficiently such that they become significantly larger than TCs in the contraction subset as shown by significant differences in the 25th, 50th, 75th, and 95th percentiles (Figure 5b). Specifically, median values for the expansion group are 962 km compared to 765 km for the contraction subset. In contrast, TC intensity shows no such significant differences between the expansion and contraction subsets with the majority of cases in both subsets showing significant weakening (Figures 5c and 5d). Examination of environmental differences suggests that the movement of TCs into a significantly more baroclinic environment by ET end is associated with larger TC outer size expansion given the differences between the expansion and contraction subsets in the 25th, 50th, 75th, and 95th percentiles (Figures 5e and 5f). Last, there are minimal differences in tropical development (i.e., maximum potential intensity) between the two subsets (Figures 5g and 5h). In their totality, these results suggest those TCs that are both smaller at ET start and subsequently move into more strongly baroclinic environments are associated with significant outer size expansion during ET.

4. Summary

This study examined how TC outer size and structure change in response to ET, and the environmental and TC characteristics associated with these changes in outer winds. Our results suggest that most TCs do not show significant changes in lower-tropospheric TC outer winds until after ET end. Our results suggest that TCs increasingly lose memory of their lower-tropospheric outer wind field size at ET start with increasing time. This memory loss is associated with initially small TCs typically undergoing the largest size growth during ET. A comparison of those minority of TCs that expand and contract in outer size during ET shows that the former subset exhibits a broad expansion of azimuthal-mean outer winds beginning in the lower troposphere at mid-ET. Thereafter, the TC outer winds continue to strengthen and build upwards into the midtroposphere. This lower-tropospheric azimuthal-mean broadening of winds is associated with increasing asymmetries concentrated downstream of those TCs in the expansion subset.

More broadly, the weakening of TC inner-core winds and subsequent expansion of outer region winds, especially after ET end, has implications for hazards. Specifically, hazards may change from concentrated wind and storm surge damage near the TC center before ET to a broader footprint of storm surge and tornadoes concentrated downstream of the TC by ET end given the sensitivity of the latter two parameters to TC outer size (Lin et al., 2014; Paredes et al., 2021).We also expect hazards to become concentrated downstream by ET end in association with the asymmetric expansion of the TC wind field as shown previously. Knowledge of the TC and environmental characteristics associated with these TC outer wind field changes may prove useful for anticipating these hazards changes, especially given that strongly expanding cases tend to impact the United States east coast more frequently.

Figure 5. Histogram with box-and-whiskers plot showing r_6 (km) at (a) ET start and (b) end, minimum sea-level pressure (hPa) at (c) ET start and (d) end, 700-hPa Eady growth rate (day^{-1}) at (e) ET start and (f) end, and potential intensity (hPa) at (g) ET start and (h) end for the expansion and contraction subsets. The median is shown by the vertical line near the center of each box, while the interquartile range is shown by the box perimeter. The notches show the 95% confidence interval of the median, while the stars denote the 5th and 95th percentiles. The lower and upper whiskers show the first datum above $q_1-1.5(q_3-q_1)$ and below $q_1 + 1.5(q_3-q_1)$, respectively. The light and dark gray thick outlines and shading for the box-and-whiskers statistics denote significant differences between the expansion and contraction subsets at the 10% and 5% levels, respectively. The dashed green vertical line shows the threshold for baroclinic development from Hart and Evans (2001).

19448007, 2025, 5, Downloaded from https://agupubs.onlinelibrary.wiley.com/doi/10.1029/2024GL111703 by University Of Oklahoma, Wiley Online Library on [04/03/2025]. See the Terms and Conditions (https://onlinelibrary.wiley.com/terms-and-conditions) on Wiley Online Library for rules of use; OA articles are governed by the applicable Creative Commons License

Data Availability Statement

TC track data were provided by the NHC, and are available at https://www.nhc.noaa.gov/data/hurdat/hurdat2-1851-2022-050423.txt (Landsea & Franklin, 2013). TC wind data were obtained from the ERA-5 provided by the ECMWF, and are available at https://rda.ucar.edu/datasets/ds633.0/ (Hersbach et al., 2020). Reanalysis TC center locations were identified using a vortex recentering algorithm available at https://doi.org/10.5281/zenodo.266194 (Brammer, 2017). Potential intensity calculations were performed using PyPI, v1.3 available at http://doi.org/10.5281/zenodo.3985975 (Gilford, 2020, 2021). All figures were made using Matplotlib, version 3.6.3, available under the Matplotlib license at https://matplotlib.org/ (Caswell et al., 2023; Hunter, 2007).

Acknowledgments

Dzuy Nguyen is supported by NSF AGS-2028151 and funding from the Honors College at the University of Oklahoma. Benjamin Schenkel is supported by NSF AGS-2028151 and the NOAA/Office of Oceanic and Atmospheric Research under the NOAA-University of Oklahoma Cooperative Agreement #NA21OAR4320204, U.S. Department of Commerce. The authors would like to thank Clark Evans (UW-Milwaukee) for helpful discussions regarding the Eady growth rate calculations and cyclone phase space. We would also like to thank two reviewers, Suzana Camargo (Columbia), Kayla Wheeler (OU), David Parsons (OU), Steven Cavallo (OU), Kim Wood (Arizona), Robert Hart (FSU), Dan Chavas (Purdue), and Christopher Landsea (NOAA) for constructive conversations.

References

Abraham, J., Strapp, J. W., Fogarty, C., & Wolde, M. (2004). Extratropical transition of Hurricane Michael: An aircraft investigation. *Bulletin America Meteorology Social*, *85*(9), 1323–1340. https://doi.org/10.1175/bams-85-9-1323

Benjamini, Y., & Hochberg, Y. (1995). Controlling the false discovery rate: A practical and powerful approach to multiple testing. *Journal of the Royal Statistical Society*, *57*(1), 289–300. https://doi.org/10.1111/j.2517-6161.1995.tb02031.x

Bian, G.-F., Nie, G.-Z., & Qiu, X. (2021). How well is outer tropical cyclone size represented in the ERA5 reanalysis dataset? *Atmospheric Research*, *249*, 105339. https://doi.org/10.1016/j.atmosres.2020.105339

Bieli, M., Camargo, S. J., Sobel, A. H., Evans, J. L., & Hall, T. (2019a). A global climatology of extratropical transition. Part I: Characteristics across basins. *Journal of Climate*, *32*(12), 3557–3582. https://doi.org/10.1175/jcli-d-17-0518.1

Bieli, M., Camargo, S. J., Sobel, A. H., Evans, J. L., & Hall, T. (2019b). A global climatology of extratropical transition. Part II: Statistical performance of the cyclone phase space. *Journal of Climate*, *32*(12), 3583–3597. https://doi.org/10.1175/jcli-d-18-0052.1

Bister, M., & Emanuel, K. A. (2002). Low frequency variability of tropical cyclone potential intensity 1. Interannual to interdecadal variability. *Journal of Geophysical Research*, *107*(D24), ACL–26. https://doi.org/10.1029/2001jd000776

Brammer, A. (2017). Tropical cyclone vortex tracker [Software]. https://doi.org/10.5281/zenodo.266194

Caswell, T. A., Lee, A., Droettboom, M., de Andrade, E. S., Hoffman, T., Klymak, J., et al. (2023). matplotlib/matplotlib: Rel: v3.6.3 [Software]. https://zenodo.org/records/7527665

Chan, K., & Chan, J. (2018). The outer-core wind structure of tropical cyclones. *Journal of the Meteorological Society of Japan*, *96*(4), 297–315. https://doi.org/10.2151/jmsj.2018-042

Chavas, D. R., Lin, N., & Emanuel, K. (2015). A Model for the complete radial structure of the tropical cyclone wind field. Part I: Comparison with observed structure. *Journal of the Atmospheric Sciences*, *72*(9), 3647–3662. https://doi.org/10.1175/jas-d-15-0014.1

Chavas, D. R., Reed, K. A., & Knaff, J. A. (2017). Physical understanding of the tropical cyclone wind-pressure relationship. *Nature Communications*, *8*(1), 1360. https://doi.org/10.1038/s41467-017-01546-9

Chavas, D. R., & Vigh, J. (2014). QSCAT-R: The QuikSCAT tropical cyclone radial structure dataset. *NCAR Tech. Note*, *TN-5131STR*, 22. https://verif.rap.ucar.edu/tcdata/quikscat/dataset/index.php

Cocks, S., & Gray, W. (2002). Variability of the outer wind profiles of western North Pacific typhoons: Classifications and techniques for analysis and forecasting. *Monthly Weather Review*, *130*(8), 1989–2005. https://doi.org/10.1175/1520-0493(2002)130<1989:votowp>2.0.co;2

Davis, C., Snyder, C., & Didlake, A. C. (2008). A vortex-based perspective of eastern Pacific tropical cyclone formation. *Monthly Weather Review*, *136*(7), 2461–2477. https://doi.org/10.1175/2007mwr2317.1

Emanuel, K. (1986). An air-sea interaction theory for tropical cyclones. Part I: Steady-state maintenance. *Journal of the Atmospheric Sciences*, *43*(6), 585–604. https://doi.org/10.1175/1520-0469(1986)043<0585:aasitf>2.0.co;2

Evans, C., & Hart, R. (2008). Analysis of the wind field evolution associated with the extratropical transition of Bonnie (1998). *Monthly Weather Review*, *136*(6), 2047–2065. https://doi.org/10.1175/2007mwr2051.1

Evans, C., Wood, K. M., Aberson, S. D., Archambault, H. M., Milrad, S. M., Bosart, L. F., et al. (2017). The extratropical transition of tropical cyclones. Part I: Cyclone evolution and direct impacts. *Monthly Weather Review*, *145*(11), 4317–4344. https://doi.org/10.1175/mwr-d-17-0027.1

Franklin, J., Black, M., & Valde, K. (2003). GPS dropwindsonde wind profiles in hurricanes and their operational implications. *Weather and Forecasting*, *18*(1), 32–44. https://doi.org/10.1175/1520-0434(2003)018<0032:gdwpih>2.0.co;2

Galarneau, T. J., & Davis, C. A. (2013). Diagnosing forecast errors in tropical cyclone motion. *Monthly Weather Review*, *141*(2), 405–430. https://doi.org/10.1175/mwr-d-12-00071.1

Galarneau, T. J., Davis, C. A., & Shapiro, M. A. (2013). Intensification of Hurricane Sandy (2012) through extratropical warm core seclusion. *Monthly Weather Review*, *141*(12), 4296–4321. https://doi.org/10.1175/mwr-d-13-00181.1

Gilford, D. M. (2020). pyPI: Potential Intensity Calculations in Python, pyPI v1.3 [Software]. https://doi.org/10.5281/zenodo.3985975

Gilford, D. M. (2021). pyPI (v1. 3): Tropical cyclone potential intensity calculations in Python [Software]. *Geoscientific Model Development*, *14*(5), 2351–2369. https://doi.org/10.5194/gmd-14-2351-2021

Haarsma, R. J., Hazeleger, W., Severijns, C., De Vries, H., Sterl, A., Bintanja, R., et al. (2013). More hurricanes to hit Western Europe due to global warming. *Geophysical Research Letters*, *40*(9), 1783–1788. https://doi.org/10.1002/grl.50360

Hart, R. (2003). A cyclone phase space derived from thermal wind and thermal asymmetry. *Monthly Weather Review*, *131*(4), 585–616. https://doi.org/10.1175/1520-0493(2003)131<0585:acpsdf>2.0.co;2

Hart, R., & Evans, J. (2001). A climatology of the extratropical transition of Atlantic tropical cyclones. *Journal of Climate*, *14*(4), 546–564. https://doi.org/10.1175/1520-0442(2001)014<0546:acotet>2.0.co;2

Hart, R., Evans, J. L., & Evans, C. (2006). Synoptic composites of the extratropical transition life cycle of North Atlantic tropical cyclones: Factors determining post transition evolution. *Monthly Weather Review*, *134*(2), 553–578. https://doi.org/10.1175/mwr3082.1

Hart, R., Maue, R., & Watson, M. (2007). Estimating local memory of tropical cyclones through MPI anomaly evolution. *Monthly Weather Review*, *135*(12), 3990–4005. https://doi.org/10.1175/2007mwr2038.1

Hersbach, H., Bell, B., Berrisford, P., Hirahara, S., Horányi, A., Muñoz-Sabater, J., et al. (2020). The ERA5 global reanalysis [Dataset]. *Quarterly Journal of the Royal Meteorological Society*, *146*(730), 1999–2049. https://doi.org/10.1002/qj.3803

Hodges, K., Cobb, A., & Vidale, P. L. (2017). How well are tropical cyclones represented in reanalysis datasets? *Journal of Climate*, *30*(14), 5243–5264. https://doi.org/10.1175/jcli-d-16-0557.1

Hoskins, B. J., & Valdes, P. J. (1990). On the existence of storm-tracks. *Journal of the Atmospheric Sciences*, *47*(15), 1854–1864. https://doi.org/10.1175/1520-0469(1990)047<1854:oteost>2.0.co;2

Hunter, J. D. (2007). Matplotlib: A 2D graphics environment [Software]. *Computer Science and Engineering*, *9*(3), 90–95. https://doi.org/10.1109/mcse.2007.55

Jones, S. C., Harr, P. A., Abraham, J., Bosart, L. F., Bowyer, P. J., Evans, J. L., et al. (2003). The extratropical transition of tropical cyclones: Forecast challenges, current understanding, and future directions. *Weather Forecasting*, *18*(6), 1052–1092. https://doi.org/10.1175/1520-0434(2003)018<1052:tetotc>2.0.co;2

Klein, P., Harr, P., & Elsberry, R. (2000). Extratropical transition of western North Pacific tropical cyclones: An overview and conceptual model of the transformation stage. *Weather and Forecasting*, *15*(4), 373–395. https://doi.org/10.1175/1520-0434(2000)015<0373:etownp>2.0.co;2

Klotzbach, P. J., Bell, M. M., Bowen, S. G., Gibney, E. J., Knapp, K. R., & III, Schreck, C. J. (2020). Surface pressure a more skillful predictor of normalized hurricane damage than maximum sustained wind. *Bulletin America Meteorology Social*, *101*(6), E830–E846. https://doi.org/10.1175/bams-d-19-0062.1

Knaff, J. A., Longmore, S. P., & Molenar, D. A. (2014). An objective satellite-based tropical cyclone size climatology. *Journal of Climate*, *27*(1), 455–476. https://doi.org/10.1175/jcli-d-13-00096.1

Landsea, C. W., & Franklin, J. L. (2013). Atlantic hurricane database uncertainty and presentation of a new database format [Dataset]. *Monthly Weather Review*, *141*(10), 3576–3592. https://doi.org/10.1175/mwr-d-12-00254.1

Lin, N., Lane, P., Emanuel, K. A., Sullivan, R. M., & Donnelly, J. P. (2014). Heightened hurricane surge risk in northwest Florida revealed from climatological-hydrodynamic modeling and paleorecords reconstruction. *Journal of Geophysical Research*, *119*(14), 8606–8623. https://doi.org/10.1002/2014jd021584

Liu, M., Vecchi, G. A., Smith, J. A., & Murakami, H. (2017). The present-day simulation and twenty-first-century projection of the climatology of extratropical transition in the North Atlantic. *Journal of Climate*, *30*(8), 2739–2756. https://doi.org/10.1175/jcli-d-16-0352.1

Loridan, T., Scherer, E., Dixon, M., Bellone, E., & Khare, S. (2014). Cyclone wind field asymmetries during extratropical transition in the western North Pacific. *Journal of Applied Meteorology and Climatology*, *53*(2), 421–428. https://doi.org/10.1175/jamc-d-13-0257.1

Marchok, T. P. (2002). How the NCEP tropical cyclone tracker works. In *25th Conf. on Hurricanes and Tropical Meteorology*.

Merrill, R. (1984). A comparison of large and small tropical cyclones. *Monthly Weather Review*, *112*(7), 1408–1418. https://doi.org/10.1175/1520-0493(1984)112<1408:acolas>2.0.co;2

Murakami, H. (2014). Tropical cyclones in reanalysis data sets. *Geophysical Research Letters*, *41*(6), 2133–2141. https://doi.org/10.1002/2014gl059519

Paredes, M., Schenkel, B. A., Edwards, R., & Coniglio, M. (2021). Tropical cyclone outer size impacts the number and location of tornadoes. *Geophysical Research Letters*, *48*(24), e2021GL095922. https://doi.org/10.1029/2021gl095922

Quinting, J. F., Bell, M. M., Harr, P. A., & Jones, S. C. (2014). Structural characteristics of T-PARC Typhoon Sinlaku during its extratropical transition. *Monthly Weather Review*, *142*(5), 1945–1961. https://doi.org/10.1175/mwr-d-13-00306.1

Sarro, G., & Evans, C. (2022). An updated investigation of post-transformation intensity, structural, and duration extremes for extratropically transitioning North Atlantic tropical cyclones. *Monthly Weather Review*, *150*(11), 2911–2933. in press. https://doi.org/10.1175/mwr-d-22-0088.1

Schenkel, B. A., Edwards, R., & Coniglio, M. (2020). A climatological analysis of ambient deep-tropospheric vertical wind shear impacts upon tornadic supercells in tropical cyclones. *Weather and Forecasting*, *35*(5), 2033–2059. https://doi.org/10.1175/waf-d-19-0220.1

Schenkel, B. A., & Hart, R. (2012). An examination of tropical cyclone position, intensity, and intensity life cycle within atmospheric reanalysis datasets. *Journal of Climate*, *25*(10), 3453–3475. https://doi.org/10.1175/2011jcli4208.1

Schenkel, B. A., & Hart, R. (2015a). An analysis of the environmental moisture impacts of western North Pacific tropical cyclones. *Journal of Climate*, *28*(7), 2600–2622. https://doi.org/10.1175/jcli-d-14-00213.1

Schenkel, B. A., & Hart, R. (2015b). An examination of the thermodynamic impacts of western North Pacific tropical cyclones on their tropical tropospheric environment. *Journal of Climate*, *28*(19), 7529–7560. https://doi.org/10.1175/jcli-d-14-00780.1

Schenkel, B. A., Lin, N., Chavas, D., Oppenheimer, M., & Brammer, A. (2017). Evaluating outer tropical cyclone size in reanalysis datasets using QuikSCAT data. *Journal of Climate*, *30*(21), 8745–8762. https://doi.org/10.1175/jcli-d-17-0122.1

Schenkel, B. A., Lin, N., Chavas, D., Vecchi, G., Oppenheimer, M., & Brammer, A. (2018). The lifetime evolution of outer tropical cyclone size. *Journal of Climate*, *31*(19), 7985–8004. https://doi.org/10.1175/jcli-d-17-0630.1

Slocum, C. J., Razin, M. N., Knaff, J. A., & Stow, J. P. (2022). Does ERA5 mark a new era for resolving the tropical cyclone environment? *Journal of Climate*, *35*(21), 3547–3564. https://doi.org/10.1175/jcli-d-22-0127.1

Thorncroft, C., Hoskins, B., & McIntyre, M. (1993). Two paradigms of baroclinic-wave life-cycle behaviour. *Quarterly Journal of the Royal Meteorological Society*, *119*(509), 17–55. https://doi.org/10.1002/qj.49711950903

Torn, R. D., & Snyder, C. (2012). Uncertainty of tropical cyclone best-track information. *Weather and Forecasting*, *27*(3), 715–729. https://doi.org/10.1175/waf-d-11-00085.1

Ventura, V., Paciorek, C. J., & Risbey, J. S. (2004). Controlling the proportion of falsely rejected hypotheses when conducting multiple tests with climatological data. *Journal of Climate*, *17*(22), 4343–4356. https://doi.org/10.1175/3199.1

Weatherford, C., & Gray, W. (1988). Typhoon structure as revealed by aircraft reconnaissance. Part I: Data analysis and climatology. *Monthly Weather Review*, *116*(5), 1032–1043. https://doi.org/10.1175/1520-0493(1988)116<1032:tsarba>2.0.co;2

Yanase, W., Shimada, U., & Takamura, N. (2020). Large-scale conditions for reintensification after the extratropical transition of tropical cyclones in the western North Pacific Ocean. *Journal of Climate*, *33*(23), 10039–10053. https://doi.org/10.1175/jcli-d-20-0013.1

19448007, 2025, 5, Downloaded from https://agupubs.onlinelibrary.wiley.com/doi/10.1029/2024GL111703 by University Of Oklahoma, Wiley Online Library on [04/03/2025]. See the Terms and Conditions (https://onlinelibrary.wiley.com/terms-and-conditions) on Wiley Online Library for rules of use; OA articles are governed by the applicable Creative Commons License